DURABILITY OF BLENDED CEMENT CONCRETE STRUCTURAL ELEMENTS OF HIGHER WATER-BINDER RATIO AGAINST CHLORIDE AND CARBONATION ATTACK

R.N. Swamy* and A.K. Suryavanshi

Department of Mechanical Engineering, University of Sheffield
Mappin Street, Sheffield, S1 3JD, U.K.

الخلاصـة :

ندرس في هذا البحث نفاذية الكلورايد في شريحة خرسانية مُقوّاه تحتوي على خليط معدنيات ونسبة عالية من الماء والماسك (water-binder w/b) تصل إلى (٠,٦)، ونختبر في هذا البحث أثر وفعالية خليط المعدنيات في مقاومة نفاذ الكلورايد عند استعمالها مقرونة بنسبة عاليـة مـن المـاء والماسك. حيث اختبرنا شريحة خرسانية ذات نسبة قدرهـا (٠,٦) تحتوي على رماد وحبيبـات كربونية إضافة إلى السيليكا وذلك بتعريضها إلى محلول تركيزه (٤٪) من كلوريد الـصـوديـوم ومن ثم تجفيفها بشكل دوري وذلك لمحاكاة أثر الكربنة على الخرسانة التي تحتوي على الكلورايد. وقد قورنت هذه النتائج مع شريحة خرسانية لاتحتوي على أية إضافات تَمَّ تعريضها لنفس الظروف التجريبية. وأظهرت هذه النتائج أنّه خلال طبقة سطحية قدرها (٢٠-٢٢ ملم) فإنَّ الخرسانة التي تحتوي على خليط المعدنيات كانت أقل تأثراً من الخرسانة التي لاتحتوي على ذات الخليط ولها ذات النسبة من الماء والماسك. وكذلك في أعماق الخرسانة وجدنا أن الخرسانة التي تحتوي على الخليط المعدني أظهرت مقاومة ملحوظة وتفوق تلك التي للخرسانة التي لاتحتوي على الخليط وذلك لنسب ماء / ماسك قدرها (٠,٤٥) و(٠,٦٠) وظهر من هذا البحث أن الإضافات المعدنية لها نتائج إيجابية في مقاومة التلف للتركيب الخرساني .

---

* To whom correspondence should be addressed.

ABSTRACT

The paper presents data on the extent of chloride penetration into reinforced concrete slabs made with mineral admixtures and a relatively high water–binder (w/b) ratio of 0.60. The aim is to examine the role and effectiveness of mineral admixtures in resisting chloride penetration when used in conjunction with high w/b ratios. For this purpose, concrete slabs with w/b ratio of 0.60 and containing fly ash, ground granulated blast furnace slag, and silica fume were exposed to cyclic ponding and drying with 4% sodium chloride solution over a period of two years. The slabs were then exposed to a drying environment to simulate the effect of carbonation on the chloride contaminated concrete. The results are compared with plain cement concrete slabs with w/b ratios of 0.45 and 0.60, and exposed to similar environment.

The results show that although the chloride penetration into the top 20 to 25 mm surface layers of the slab was very high, irrespective of the w/b ratio, the slabs with mineral admixtures, with the exception of fly ash, showed reduced chloride concentration compared to the control slab with the same w/b ratio but without mineral admixtures. However, at greater depths, all the slabs with blended cement concrete, showed remarkable resistance to chloride penetration, superior to that of plain cement concrete slabs made with w/b ratios of 0.45 and 0.60. The data presented here demonstrate that incorporating mineral admixtures, even at high w/b ratios, has a very positive effect in reducing damage to real structural elements. The results also emphasize that, in heavily salt-laden environments, even a w/b ratio of 0.45 will not prevent chloride penetration into the surface layers of the concrete.

Keywords: Long-term Durability, Mineral Admixtures, Atmospheric Carbonation, Chloride Penetration.

DURABILITY OF BLENDED CEMENT CONCRETE STRUCTURAL ELEMENTS OF HIGHER WATER–BINDER RATIO AGAINST CHLORIDE AND CARBONATION ATTACK

INTRODUCTION

It is now universally recognized that the water–binder (w/b) ratio is one of the key parameters that influences the penetration of chloride ions into the concrete. For structures exposed to severe chloride-laden environments, such as coastal and marine structures and bridge decks exposed to deicing salts, current building codes therefore recommend, quite sensibly, low w/b ratios which will lead to high quality concretes. Low w/b ratios by themselves, however, are unlikely to lead to corrosion-free structures since all concretes irrespective of their w/b ratios, will crack at very low strains due to stresses arising from external loads or from fabrication processes such as drying shrinkage and thermal movements. Long-term durability of concrete elements will, therefore, depend not merely on the w/b ratio but also on other factors such as the presence of mineral admixtures in the mix constituents, crack control, fabrication processes, early age protection of the concrete from a drying environment, and microclimate in the immediate vicinity of the structure. It is clear that a global design strategy that integrates material characteristics and structural performance is necessary to ensure the durability service life of structures exposed to aggressive environments [1–4].

On the other hand, it is also now recognized that, the incorporation in concrete of pozzolanic and cementitious mineral admixtures such as fly ash (FA), ground granulated blast furnace slag (GGBFS), and silica fume (SF) can substantially improve the physical, chemical and mechanical properties of the resulting concrete [5–8]. The presence of these siliceous admixtures in concrete has been shown to enhance the quality of microstructure, which leads directly to increased protection against degradation and deterioration caused by chloride penetration, sulfate attack, and alkali–aggregate reaction. Further, the addition of these pozzolanic materials to concrete also reduces the thermal, plastic, and shrinkage cracking often regarded as one of the main causes of deterioration of plain cement concrete structural elements. However, the most significant advantage derived by incorporating these pozzolanic materials in concrete is their enhanced resistance to the penetration of chlorides from an external environment [5, 8]. Thus, in rationally designed blended cement concrete structures, the chances of deterioration as a result of reinforcement steel corrosion are significantly lower compared to those quite often noticed in plain cement concrete structures. However, from the literature, it is also apparent that the blended cement concrete structures show wide variations in their long-term durability performance. This may be attributed to the variations in the physical, chemical, and mineralogical properties of the mineral admixtures as a result of the industrial processes related to their production, or due to variations in the properties of the raw materials used, or both. The mix proportioning methods, and the curing regimes adopted, also significantly control the long-term durability performance of the resulting concrete [6–9]. Hence, careful evaluation is required before deriving any conclusions on the long-term durability performance of blended cement concretes.

Due to recent widespread deterioration and degradation of plain cement concrete structures, it is common practice now to incorporate pozzolanic mineral admixtures into low water–binder ratio (0.45 and below) concretes, in order to enhance their durability, especially against chloride and atmospheric carbonation attacks. The blended cement concretes are known to derive their markedly improved resistance against the penetrating chloride and carbonation attack, mainly from the pore refinement process, in which, the coarse pores are filled with the secondary C–S–H gel, resulting in reduced porosity and permeability with a discontinuous pore structure [5]. Thus, knowing the inherent capabilities of the mineral admixtures in improving the durability of concretes with a range of w/b ratios against chloride and carbonation attack, would immensely help to enhance the quality of construction, and their durable service life. It would also help engineers to understand the role and effectiveness of mineral admixtures on the long-term durability performance of those blended cement concrete elements cast with concrete of a higher w/b ratio than that recommended in codes of practice for a given environment. It has, for example, been recently reported that ready mixed concretes delivered to sites frequently exceed the recommended w/b ratio specified in codes of practice [9]. Thus, it would be of interest to know the adverse effects onto the long-term durability of blended cement concrete elements of relatively high w/b ratio.

The aim of the study reported here is to examine the resistance to chloride penetration and carbonation of concretes containing mineral admixtures but made with a relatively high w/b ratio of 0.60. The data presented here form part of an extensive long-term study of the durability of reinforced concrete slabs made without and with various mineral admixtures and with a range of w/b ratios from 0.45 to 0.75. The focus of the data presented here is the long-term durability of concrete slabs of 0.60 w/b ratio containing cement blended with 30% FA, 65% GGBFS, or 10% SF, and the results are compared with portland cement concrete slabs without mineral admixtures and w/b ratios of 0.45 and 0.60.

EXPERIMENTAL

Test Slabs

In the present experimental investigation, the results of three reinforced concrete slabs of 0.6 w/b ratio incorporating FA, GGBFS, and SF are used. For purposes of comparison, the data from a plain cement concrete slab of 0.60 w/b ratio (control slab) along with another plain cement concrete slab cast with a concrete mix of 0.45 w/b ratio are also included. The concrete mix with 0.45 w/b ratio generally simulates the concrete mix normally recommended in codes of practice for aggressive environmental conditions. In the blended cement concrete slabs, the cement was replaced with the mineral admixture on a mass basis while, the aggregate and water contents were maintained constants for all the slabs. Thus, for all the slabs the total cementitious content was maintained at 350 kg m^{-3} and the aggregate/cementitious ratio was 5.21. Other data on the concrete mixtures used for making test slabs are given in the Table 1.

In all the slabs, ordinary portland cement (OPC) containing 9% tri-calcium aluminate (C_3A) and 7% tetra calcium aluminoferrite (C_4AF) by mass was used. Table 2 gives the oxide composition of the cement and the mineral admixtures used in the present investigation. The FA used in the present investigation is a low calcium FA conforming to Class F of ASTM C 618 [10]. The surface area of the FA was such that it satisfied the BS 3892 on the 45 μm sieve [11]. The Blaine surface area for cement was 345 m^2 kg^{-1}, and for GGBFS, it was 417 m^2 kg^{-1}, while for the SF the mean particle size varied between 0.1 and 0.2 μm.

To obtain a uniform mix and also to reduce bleeding during setting, the following concrete mixing procedure was adopted. To start with, all of the coarse aggregates along with 1/3rd of the total mixing water were added to the mixer, and they were mixed for 60 seconds. The fine aggregates, cement and the mineral admixtures were then added, and were mixed for 30 seconds. Finally, the remaining 2/3rd of mixing water was added, and they were mixed for another 90 seconds. No plasticizers were used in the concrete mix. The slump for the concrete mixtures was measured immediately after mixing. The plain cement concretes of 0.60 and 0.45 w/b ratio showed slumps of 80 mm and 30 mm respectively while, the 30% FA, 65% GGBFS, and 10% SF concretes showed slumps of 160 mm, 115 mm, and 25 mm respectively. The concrete was placed into the moulds in three layers, and each layer was vibrated with an internal vibrator until no air bubbles were seen emerging from the concrete.

After casting, the slabs were covered by polyethylene sheets for 24 hours. The slabs were then cured by ponding water on the top surface for 6 days, then sponge dried, demolded, and exposed to laboratory curing environment for 21 days, prior to exposure to chlorides.

Table 1. Concrete Mixtures Used for Making Test Slabs.

Slab type	w/b ratio	Size (mm)	Special features
OPC/65% GGBFS	0.60	1000×500×150	65% cement replacement by GGBFS by mass
OPC/30% FA	0.60	1000×500×150	30% cement replacement by FA by mass
OPC/10% SF	0.60	1000×500×150	10% cement replacement by SF by mass
OPC	0.60	1000×1000×150	Plain cement concrete slab
OPC	0.45	1000×1000×150	As above

Table 2. Oxide Analyses of Cement and Mineral Admixtures.

Cementitious material	SiO_2	Al_2O_3	Fe_2O_3	CaO	MgO	K_2O	Na_2O
Cement	21.09	4.84	2.39	63.85	3.32	1.24	0.29
GGBFS	34.2	11.3	1.17	41.6	8.21	0.4	0.26
FA	51.4	28.1	11.1	1.38	1.62	4.08	1.32
SF	97.0	—	—	—	—	—	—

Exposure Regime

At the time of casting, the slabs were provided with an acrylic frame of 50 mm height; this frame formed an embankment on the top surface of the slabs for ponding with salt solution. Immediately after curing all the slabs for a total of 28 days, they were exposed to a series of chloride penetration regimes, consisting of 7 days of ponding with 4% sodium chloride (NaCl) solution followed by 3 days of drying. All the slabs were thus exposed to a total of 70 cycles in steps of 10, 20, 50, and 70 cycles. For each cycle of exposure freshly prepared NaCl solution was used. Short time intervals of a few days occurred between 10 and 20, and 20 and 50 cycles, while a longer time interval of about one and half years was deliberately maintained between 50 and 70 cycles in order to allow the redistribution of chlorides into the concrete and also to carbonate the concrete. After completion of the 70 cycles of ponding and drying, the slabs were left exposed to a laboratory drying environment for about two and half years in order to effect some carbonation penetration into the chloride contaminated concrete. Since carbonation ingress is a slow time-dependent process, it was felt that this period will enable some interaction to occur between carbonation and the hydration compounds of chloride-infiltrated concrete. The tests reported here were thus carried out on slabs about six years old.

Test Details

Three series of tests were carried out in this study. The first series of tests consisted of establishing the chloride profiles over the depth of the slabs. The chloride contents were determined as acid soluble chloride (percent by mass of total cementitious content) by Volhard's method, as described in BS 1881 [12]. The second series of tests consisted of X-ray diffraction (XRD), and differential thermal analyses (DTA) on the hydrated cement powders to identify the phases present. The third series consisted of phenolphthalein spray tests on freshly cored samples.

The X-ray diffraction analysis on powdered samples was carried out on a Phillips diffractometer with Cu Kα radiation ($\lambda = 154.18$ pm(1.5418 Å)) as X-ray source. The scan speed used was 2° per minute with a scan-step of 0.02°. The X-ray tube voltage and current were fixed at 50 kV and 30 mA respectively. The thermal studies were carried out on a Stanton Redcroft DTA (model 673-4). Powdered samples weighing 100 mg were used in order to make the samples representative, although this might result in thermal gradients within the sample. The samples were scanned from room temperature to 850°C with a scan speed of 10°C per minute. Powdered alumina was used as a reference material. Platinum crucibles were used as containers for both reference material and the powdered sample.

Concrete samples for the above tests were obtained by coring the slabs with a water lubricated vacuum-based Hilti core cutter to a depth varying between 105 mm and 115 mm. All the slabs were cored at six randomly selected locations to the same depth as above. The cores (25 mm diameter) thus obtained were sliced on a water-lubricated circular saw into the following depths: 0–5, 5–25, 25–45, 45–65, 65–85, and 85–105 mm. These sliced samples were then passed through a jaw crusher. The sliced samples from the same depth were mixed in order to obtain a representative sample for each slab at a given depth. The large aggregates were separated by passing the coarsely crushed samples through a 2 mm sieve. The coarsely crushed samples were finally crushed to a fine size in a heavy duty pestle and mortar. These were then passed through a 150 μm sieve and the powder was used for chloride analyses and also for XRD and DTA studies.

The third test for the depth of carbonation was performed on newly drilled 25 mm diameter cores with phenolphthalein spray. Phenolphthalein (1% in ethanol) solution was sprayed onto the freshly split cores and the carbonated depths were immediately measured.

RESULTS

1. Chloride Analyses

Figure 1 shows the acid soluble chloride profiles for all the slabs as a function of depth intervals from the surface after undergoing 70 exposure cycles, followed by a two and half years exposure to a drying environment. The plain cement concrete slab (control slab) cast with a concrete of 0.60 w/b ratio showed the presence of significant amounts of acid-soluble chlorides at all the depth intervals investigated, though the chloride content gradually decreased with increasing depths from the surface. All the slabs with mineral admixtures, that is, with FA, GGBFS, and SF showed significant reductions in chloride concentration at the 25–45 mm depth interval and beyond, compared to the control slab. However, the 30% FA slab showed a larger quantity of chloride than the control slab (0.60 w/b ratio) at the 0–5 mm and 5–25 mm depth intervals. The 10% SF slab showed the least quantity of chlorides at the 0–5 mm, and the 5–25 mm depth intervals compared to other 0.60 w/b slabs; however, all the slabs with mineral admixtures showed practically no chlorides present beyond the

45–65 mm depth interval. The plain cement concrete control slab with w/b ratio of 0.45 was very effective in controlling the chloride penetration into the surface layers of the slab up to a depth interval of 5–25 mm. However, it showed higher chloride concentration at the depth interval of 25–45 mm than the slabs with mineral admixtures and w/b ratio of 0.60. At and beyond the depth interval of 45–65 mm the plain cement concrete slab with 0.45 w/b ratio, like the slabs with mineral admixture at 0.60 w/b ratio, showed negligible amount of chloride penetration.

It is important to note here that these results emphasize that even a w/b ratio as low as 0.45, will not prevent chloride penetration into the concrete, and thus, will not give complete protection from possible corrosion of embedded steel in the long-term. Indeed, in situations where structures are exposed to salt-laden environments throughout their life, chlorides will exist at almost their safe threshold level in the surface layers within a few years of exposure to chlorides [1–4].

The presence of large amounts of chloride at the surface of the slabs might suggest the formation of a complex chloro-aluminate hydrate such as Friedel's salt ($3CaO.Al_2O_3.CaCl_2.10H_2O$). In order to fully understand the complex interactions between chlorides and the hydration compounds in concrete without and with mineral admixtures, extensive tests were carried out on XRD and DTA and these are discussed below.

2. XRD and DTA Analyses

The section below presents both the XRD and DTA results for the samples drawn from the 0–5 mm and 5–25 mm depth intervals from the 30% FA, 65% GGBFS, 10% SF, and the plain cement concrete (0.60 w/b ratio) slabs. All the XRD diffractograms presented below are plotted with an identical scale for the y-axis (number of counts), and hence they are comparable. The same is also true for the y-axis (ΔT: Temperature difference) of the DTA thermograms presented below.

2.1. 30% FA Slab

Figure 2 shows the XRD diffractograms for the samples drawn from the 0–5 mm and 5–25 mm depth intervals. The diffractogram for the 0–5 mm depth interval shows dominant maximum intensity peaks for α-quartz (SiO_2) and calcium carbonate ($CaCO_3$) in the form of calcite and vaterite. However, the maximum intensity peaks for Friedel's salt, portlandite ($Ca(OH)_2$) and ettringite ($3CaO.3CaSO_4.Al_2O_3.32H_2O$) are absent.
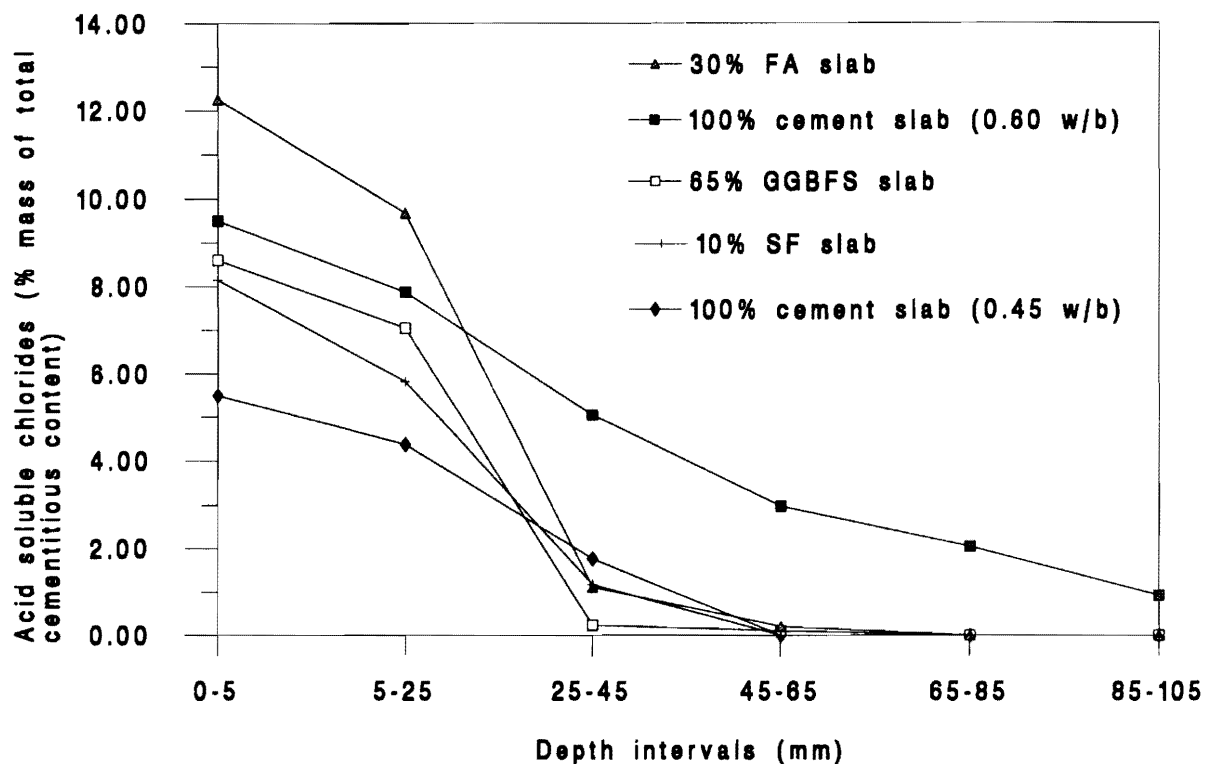

Figure 1. Acid Soluble Chlorides in Different Types of Slabs by Percentage Mass of Total Cementitious Content.

In contrast, the diffractogram for the 5–25 mm depth interval shows a dominant peak for Friedel's salt and also a fairly definite maximum intensity peak for ettringite and the absence of calcite and vaterite. A small peak for portlandite is also evident. The broader peak appearing in place of crystalline calcite appears to be due to the poorly crystalline C–S–H gel, however, it may be due to the poorly crystalline calcite.

However, the XRD results alone are inconclusive in identifying the phases present as several phases with identical d-spacing are known to exist in hydrated cements. One of them is the tetra-calcium aluminate 13-hydrate (C_4AH_{13}), a meta-stable hydrate of tri-calcium aluminate (C_3A), similar to the Friedel's salt which also has its maximum intensity peak at 790 pm [13]. Many cement chemists use thermal analyses such as DTA and differential scanning calorimetry (DSC) to make a distinction between Friedel's salt and the C_4AH_{13}. The presence of Friedel's salt is indicated through an endothermic peak centered between 300°C and 350°C (due to loss of crystalline water), with most of the reports suggesting the thermal event to be centered at or close to 350°C [14–16]. On the other hand, the presence of C_4AH_{13} results in a series of endothermic peaks centered below 300°C at 280°C, 190°C, 125°C, 90°C, and 75°C due to the gradual loss of crystalline water [17]. The presence of calcite with its maximum intensity peak at 304 pm is also inconclusive from the XRD alone, as the C–S–H gel also has its maximum intensity peak at 307 pm [13]. However, in normally hydrated portland cements, the C–S–H gel is known to be nearly amorphous, and hence, it is not expected to give a dominant response on the XRD diffractogram. On a DTA thermogram, the decomposition of well-crystalline calcite into calcium oxide (CaO) is indicated through an endothermic peak centered close to 800°C, while the amorphous calcite decomposes into CaO at relatively lower temperature than the crystalline calcite [18]. Similarly, the presence of ettringite is confirmed through an endothermic peak centered around 140°C due to the loss of crystalline water [19]. Portlandite starts dehydrating to CaO at about 400°C on a DTA thermogram, it therefore gives rise to a strong peak centered around 500°C [20]. The presence of α-quartz originating from sand is confirmed through an endothermic peak centered at 573°C, at which it transforms into β-quartz [13].

Figure 3 presents the DTA thermograms for the 0–5 mm and 5–25 mm depth intervals. In conformity with the XRD results, the thermogram for the 0–5 mm depth interval shows the endothermic peaks to indicate the presence of α-quartz (centered at 570°C) and calcite (centered at 785°C). The endothermic peak appearing around 120°C indicates the loss of free water from the sample.

On the other hand, the thermogram for the 5–25 mm depth interval shows the presence of Friedel's salt through a definite and dominant endothermic peak centered at 350°C, and also the ettringite through a well-defined endothermic peak centered at 165°C. There is no endothermic peak to indicate the presence of calcite (amorphous or crystalline), and apparently, the broader peak appearing in place of crystalline calcite in the XRD diffractogram is due to the poorly crystalline C–S–H gel. Although, the XRD diffractogram indicated the presence of portlandite by a tiny peak, the DTA thermogram failed to confirm its presence. This might be due to the thermal event related to the portlandite falling well below the sensitivity of the
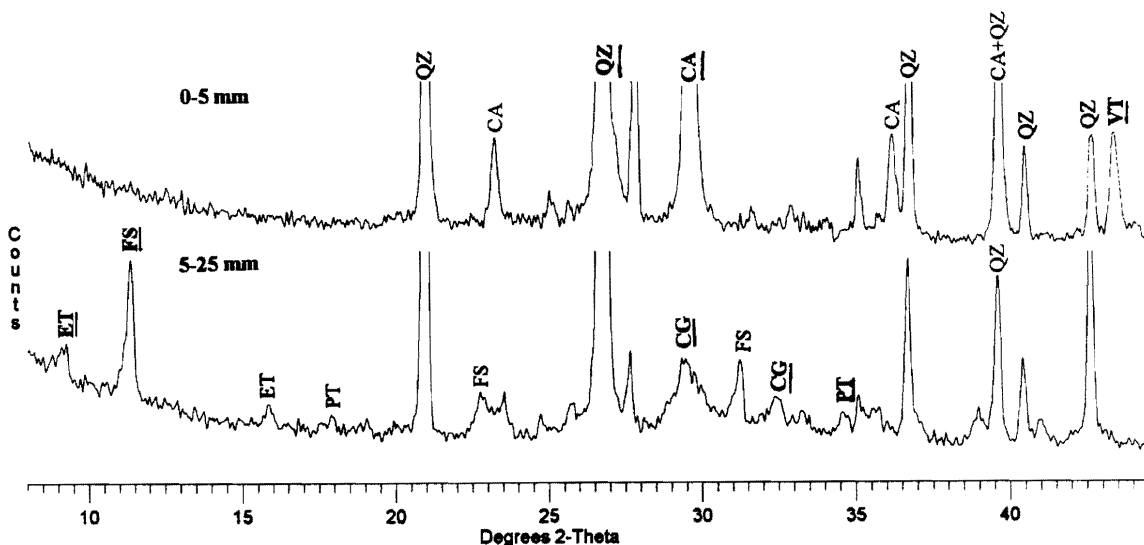

Figure 2. X-Ray Diffractograms for 30% FA Slab.
(Keys: QZ: α-Quartz, CA: Calcite, VT: Vaterite, ET: Ettringite, FS: Friedel's salt, PT: Portlandite, CG: C-S-H gel.
The keys in bold and underlined letters indicate the 100% intensity peaks).

instrument as a result of minimal amount of portlandite. An endothermic peak centered at 570°C indicates the presence of α-quartz.

From the above results it is clear that the 0–5 mm depth was carbonated while the concrete present at the 5–25 mm depth interval was free from carbonation attack. The carbonation attack at the surface is indicated by the abundantly present calcium carbonate in the form of calcite and vaterite, and the non-existence of Friedel's salt, portlandite, and ettringite which are found to be present at the 5–25 mm depth interval.

2.2. 65% GGBFS and 10% SF Slabs

Figures 4 and 5 show the XRD diffractograms for the 65% GGBFS and the 10% SF slabs respectively. Contrary to the 30% FA slab, both slabs for the 0–5 mm depth interval show the maximum intensity peaks for Friedel's salt, ettringite, calcite, vaterite, and portlandite. However, the peaks for Friedel's salt and portlandite are small.

Alternatively, the diffractograms for the 5–25 mm depth interval for both the slabs show maximum intensity peaks for Friedel's salt and portlandite, which are higher in intensities in the absence of calcite and vaterite. In both slabs, a broader peak appearing in place of the crystalline calcite appears to be due to the poorly crystalline C–S–H gel; however, it may be due to the poorly crystalline calcite.
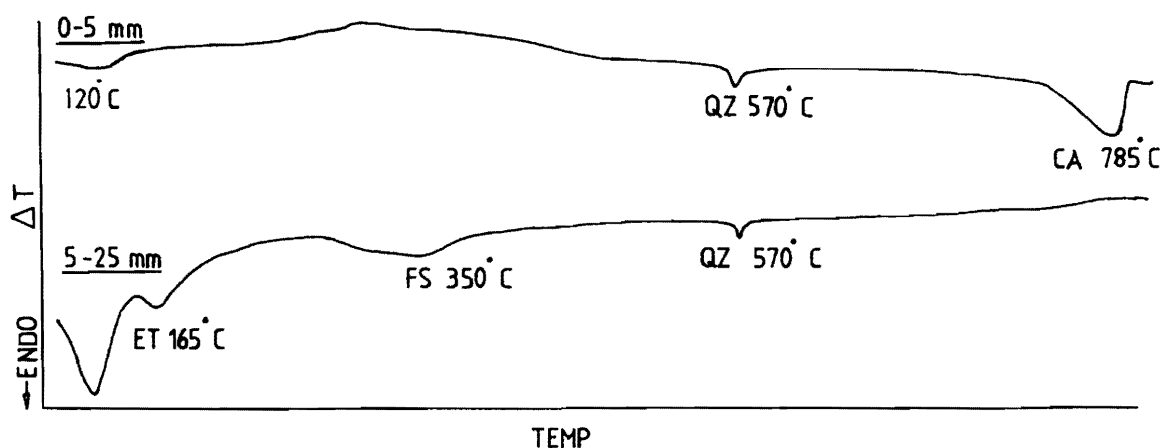

Figure 3. DTA Thermograms for 30% FA Slab.
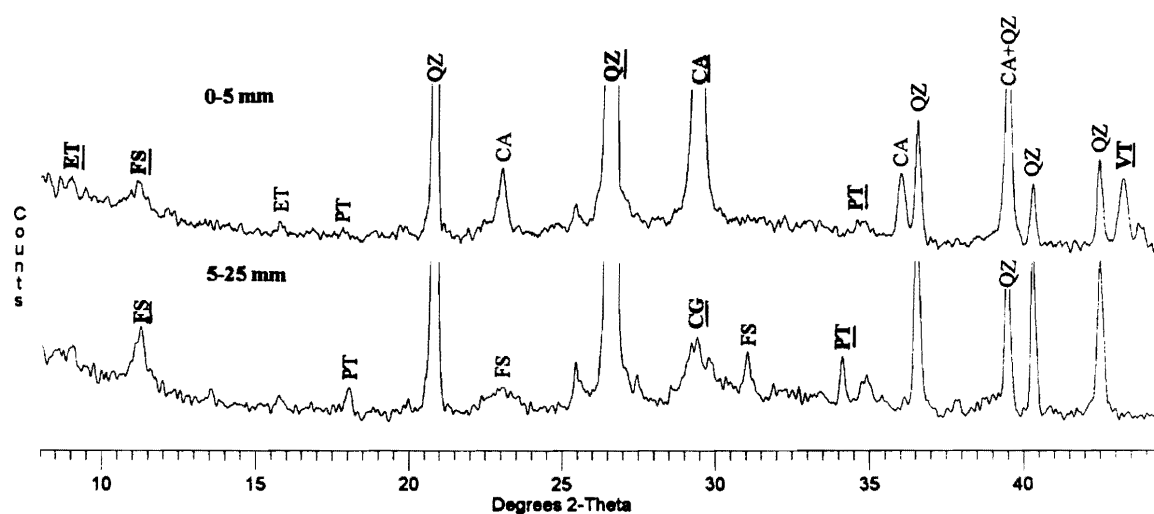(Keys: QZ: α-Quartz, CA: Calcite, ET: Ettringite, FS: Friedel's salt).

Figure 4. X-Ray Diffractograms for 65% GGBFS Slab.
(Keys: QZ: α-Quartz, CA: Calcite, VT: Vaterite, ET: Ettringite, FS: Friedel's salt, PT: Portlandite, CG: C-S-H gel.
The keys in bold and underlined letters indicate the 100% intensity peaks).

Figures 6 and 7 show the DTA thermograms for 65% GGBFS and 10% SF slabs respectively. For the 65% GGBFS slab, the thermogram for the 0–5 mm depth interval (Figure 6) shows the endothermic peaks centered at 155°C, 365°C, and at 775°C, indicating the presence of ettringite, Friedel's salt and calcite respectively. Similarly, for 10% SF slab (Figure 7), the
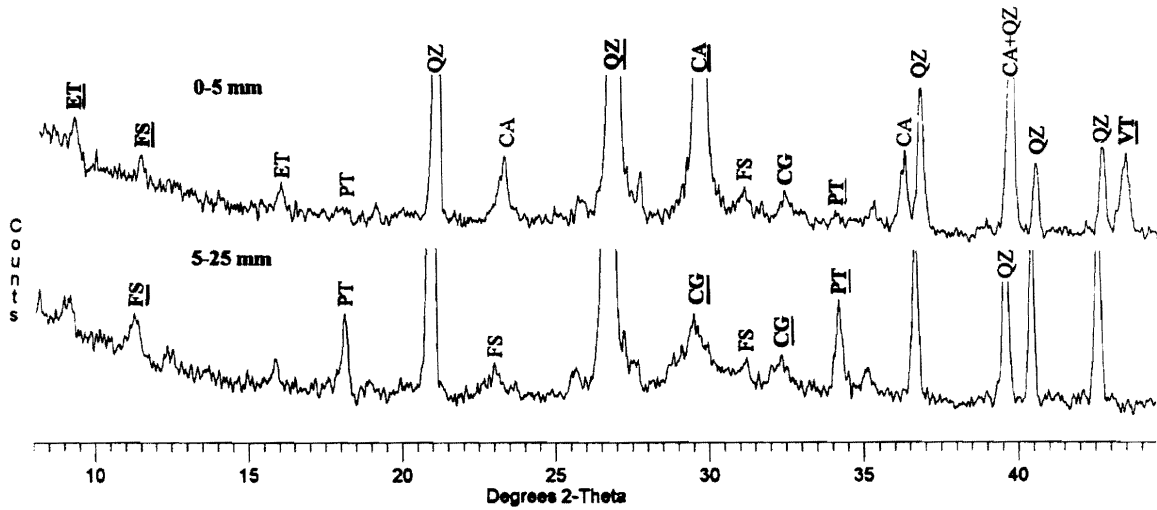

Figure 5. X-Ray Diffractograms for 10% SF Slab.
(Keys: QZ: α-Quartz, CA: Calcite, VT: Vaterite, ET: Ettringite, FS: Friedel's salt, PT: Portlandite, CG: C-S-H gel.
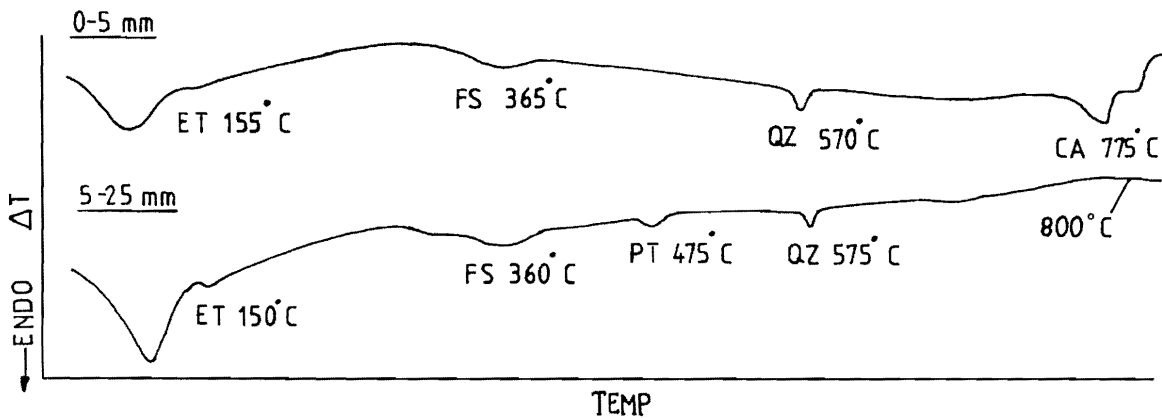*The keys in bold and underlined letters indicate the 100% intensity peaks).*

Figure 6. DTA Thermograms for 65% GGBFS Slab.
(Keys: ET: Ettringite, FS: Friedel's salt, QZ: α-Quartz, CA: Calcite, PT: Portlandite).
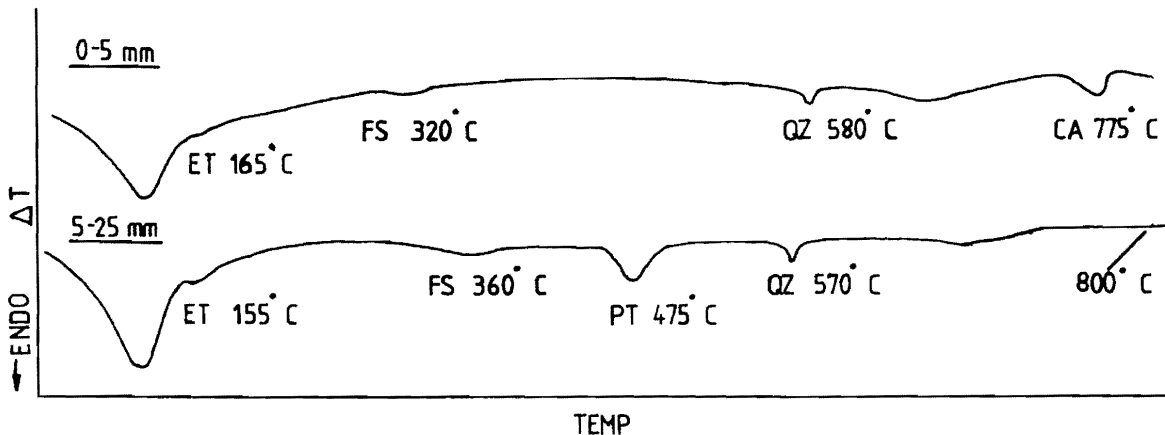

Figure 7. DTA Thermograms for 10% SF Slab.
(Keys: ET: Ettringite, FS: Friedel's salt, QZ: α-Quartz, CA: Calcite, PT: Portlandite).

thermogram for the 0–5 mm shows endothermic peaks centered at 165°C, 320°C, and 775°C indicating the presence of ettringite, Friedel's salt, and calcite respectively. For both slabs no peak is present in the DTA thermogram to indicate the presence of portlandite.

The thermogram for the 5–25 mm depth interval from the 65% GGBFS slab (Figure 6), in conformity with the XRD result, shows definite endothermic peaks centered at 360°C, 475°C, and 150°C to indicate the presence of Friedel's salt, portlandite, and ettringite respectively. The endothermic peak for Friedel's salt is relatively clear and dominant in size, compared to that for the 0–5 mm depth interval. There is no peak to indicate the presence of calcite due to carbonation of concrete, which is in conformity with the XRD results. This also suggests that the broader peak appearing in place of crystalline calcite is due to the poorly crystalline C–S–H gel.

The thermogram for the sample drawn from the 5–25 mm depth interval of the 10% SF slab (Figure 7), shows, in conformity with the XRD result, relatively clear and definite endothermic peaks for Friedel's salt (centered at 360°C), ettringite (centered at 155°C), and portlandite (475°C). Once again, in conformity with the XRD results, there is no peak to indicate the presence of calcite due to carbonation of concrete. This also suggests that the broader peak appearing in place of crystalline calcite is due to the poorly crystalline C–S–H gel.

By taking the DTA peak height as a criterion for relative evaluation of estimating the amount of calcite formed in the concrete at the 0–5 mm depth interval, it is evident that the 30% FA slab has the largest amount of calcite while, the 10% SF slab has the least. On the other hand, the amount of calcite present in the concrete sample drawn from the 0–5 mm depth interval of the 65% GGBFS slab was between the two. It is also clear that portlandite, Friedel's salt, and ettringite were present in the samples drawn at the 0–5 mm depth interval from the 65% GGBFS and 10% SF slabs, which had less calcite than the 30% FA slab at the corresponding depth interval.

2.3. Plain Cement Concrete Slab (0.60 w/b ratio)

Figure 8 presents the XRD diffractograms for the 0–5 mm and 5–25 mm depth intervals for the plain cement concrete slab made with 0.60 w/b ratio. The diffractogram for the 0–5 mm depth interval shows the existence of phases such as ettringite, Friedel's salt, and portlandite in significant proportions in the presence of both calcite and vaterite. On the other hand, the diffractogram for the 5–25 mm depth interval emphasizes the presence of portlandite in dominant proportions in the absence of calcite and vaterite. The broader peak appearing in place of the calcite peak is believed to be due to the poorly crystalline C–S–H gel or the amorphous calcite.
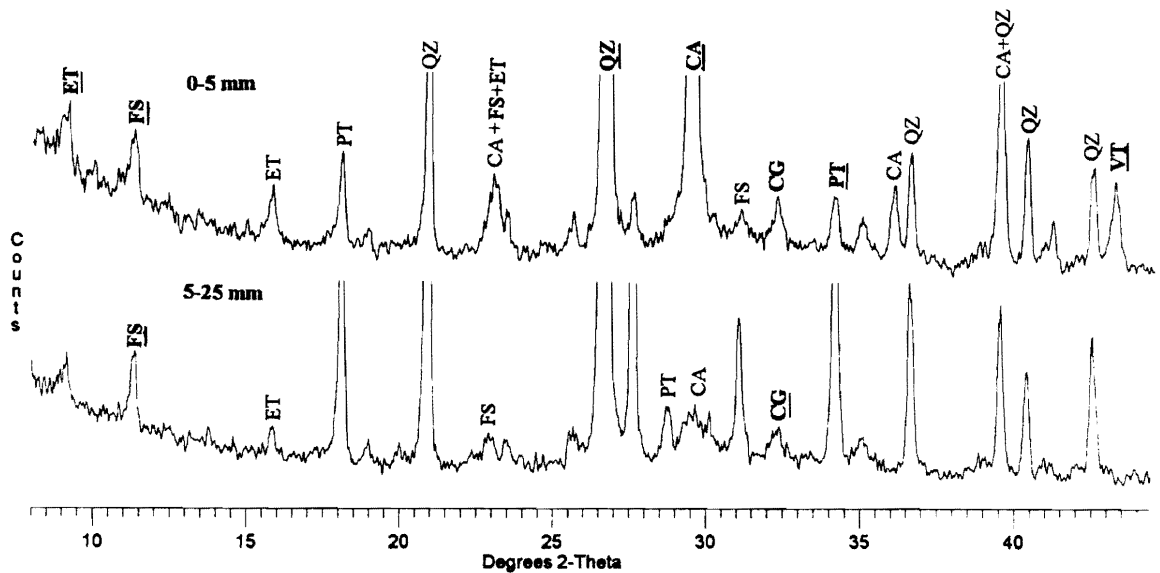

Figure 8. X-Ray Diffractograms for Plain Cement Concrete Slab.
(Keys: QZ: α-Quartz, CA: Calcite, VT: Vaterite, ET: Ettringite, FS: Friedel's salt, PT: Portlandite, CG: C-S-H gel.
The keys in bold and underlined letters indicate the 100% intensity peaks).

Figure 9 illustrates the DTA thermograms for the above depth intervals. The thermogram for the 0–5 mm depth interval shows the endothermic peaks centered at 160°C, 360°C, 480°C, and at 780°C to indicate the presence of ettringite, Friedel's salt, portlandite, and calcite respectively. The thermogram for the 5–25 mm depth interval shows clear and definite endothermic peaks for ettringite (160°C) and Friedel's salt (335°C). In accordance with the XRD results, the dominant endothermic peak centered at 485°C indicates the presence of portlandite in significant proportions. The DTA thermogram for the 5–25 mm depth interval shows a fairly dominant endothermic peak centered at 770°C to indicate the presence of amorphous calcite [18], and hence the broader endothermic peak on XRD diffractogram may be due to the amorphous calcite.

By taking the DTA peak height as a criterion, the amount of calcite formed in the concrete at the 0–5 mm depth interval of the slabs in the descending order is given as, 30% FA slab, plain cement concrete slab (0.60 w/b ratio), 65% GGBFS slab, and 10% SF slab. For the plain cement concrete slab (0.60 w/b ratio), the DTA results indicated the progress of carbonation front into the concrete at the 5–25 mm depth interval which was not observed in any of the other slabs. The results also indicated the presence of Friedel's salt, portlandite, and ettringite in dominant proportions in the concrete drawn at the 0–5 mm and 5–25 mm depth intervals from the plain cement concrete slab.

3. Phenolphthalein Spray Test

The phenolphthalein spray test showed average carbonation depths of 5 mm, 3 mm, 2.5 mm, and 1.25 mm for the 30% FA slab, control slab, (0.60 w/b ratio), 65% GGBFS slab, and 10% SF slab respectively. Thus, the entire concrete present at the 0–5 mm depth interval for the 30% FA slab was carbonated while, the concrete at the 0–5 mm depth interval for the 10% SF slab was carbonated to the least depth. Similar to the 10% SF slab, the plain cement concrete slab cast with a w/b ratio of 0.45 also showed an average carbonation depth of 1.25 mm.

DISCUSSION

Chloride Penetration

In the present investigation the slabs were subjected to repeated wetting (4% NaCl solution) and drying cycles after the initial 28 days curing. Chlorides are known to penetrate into the dry concrete by a capillary absorption mechanism. In the present case, there is a possibility for the chlorides to get transported into the concrete at the surface by capillary absorption during the beginning of the very first wetting cycle, and then every time during the beginning of the first cycle after the long-term laboratory drying period. There is also the possibility of physical transportation of chlorides into the concrete due to the flow of water through the capillary pore system depending on the permeability of concrete. However, once the slabs get saturated with moisture due to the continued wetting and drying cycles, the ionic diffusion would be the primary mechanism for the penetration of chlorides into the concrete.

As discussed earlier, the 30% FA and the 65% GGBFS slabs showed small amounts of chlorides at the 45–65 mm depth intervals. It is reported in the literature that the reinforcement steel in concrete made from OPC will be under a lower
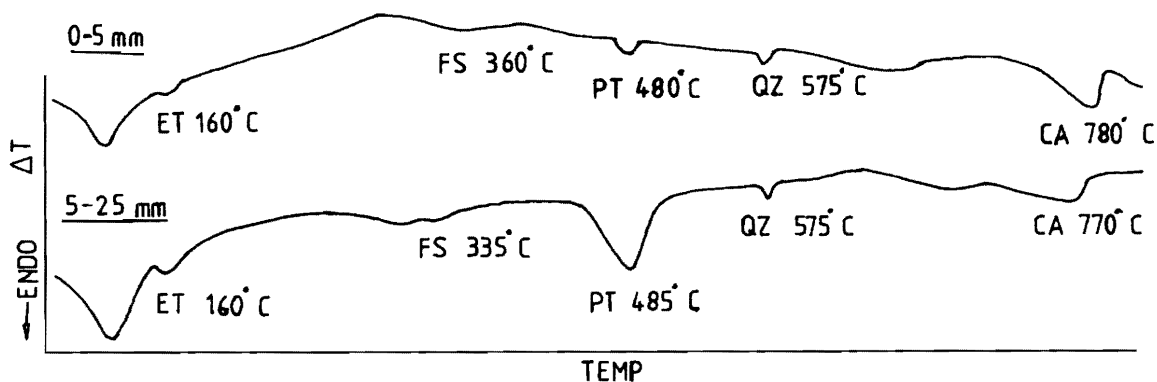

Figure 9. DTA Thermograms for Plain Cement Concrete Slab.
(Keys: ET: Ettringite, FS: Friedel's salt, QZ: α-Quartz, CA: Calcite, PT: Portlandite).

corrosion risk when the total chlorides by weight of cement are below 0.4% [21]. Assuming the above criterion also holds good for the blended cement concrete, it appears that the chlorides present at the 45–65 mm depth interval are practically insignificant. The 10% SF slab showed a total absence of chlorides at the above depth interval. In contrast, over a similar period of time, a significant amount of chlorides penetrated to greater depths (85–105 mm depth interval) for the control slab cast with a concrete mix of 0.60 w/b ratio. The above results demonstrate the advantage of blending the concretes mixes of higher w/b ratio with mineral admixtures from a view point of delaying the onset of corrosion attack on the reinforcement steel. However, for the blended cement concrete structural elements of 0.60 w/b ratio designed with less than 45 mm cover, the depth of chloride penetration is still a matter of concern from the view point of corrosion.

Over a similar period of exposure, though the blended cement concrete slabs showed large chloride contents at the surface (0–5 mm and 5–25 mm), the amount of chlorides at the 25–45 mm depth interval was less than that for the plain cement concrete slab of 0.45 w/b ratio. Thus, despite the higher w/b ratio of 0.60, the blended concrete slabs showed improved resistance to chloride penetration, particularly from the 25–45 mm depth interval onwards compared to the plain cement concrete slab of 0.45 w/b ratio. The present study once again suggests that, in blended cement concrete elements of 0.60 w/b ratio, the reinforcement steel would not be under an immediate threat from corrosion attack, provided that the structure is designed with an adequately thick cover, in conformity with the recommendations of the codes of practice for structures in aggressive chloride environments. Thus, from the above discussion it is evident that, by blending the concrete of 0.60 w/b ratio with mineral admixtures, there is a definite advantage of delaying the onset of the corrosion attack, provided the structural element is designed with an adequate cover.

The increased resistance to chloride penetration at greater depth intervals (25–45 mm) in blended cement concrete slabs is attributed to the pore refinement occurring due to the conversion of dense $Ca(OH)_2$ into secondary C–S–H gel by pozzolanic reaction. The secondary C–S–H gel, although less dense compared to the primary C–S–H gel formed in plain cements, is nevertheless reported to be effective in filling up the large capillary pores in blended cement systems [22]. The greater resistance to chloride penetration of blended cements is thus due to the generation of a discontinuous pore structure compared to that in the hydrated portland cement. The discontinuous nature of the pore structure in blended cements is also partly ascribable to a net reduction in $Ca(OH)_2$ content due to the strong pozzolanic reaction. It is reported that, the $Ca(OH)_2$ formed due to the hydration of cement in concrete generates a continuous pore structure [23]. The increased resistance to chloride penetration at greater depths may also be partly due to the possible surface interaction between the diffusing chloride ions and the pore walls as suggested by Collepardi *et al;* however, the precise nature of this interaction is not clearly understood [24].

The presence of large quantities of chlorides at the surface (0–5 mm and 5–25 mm) of the 30% FA slab is explained by the presence of relatively porous concrete at the surface. It has been reported that concrete structural elements cast by incorporating low calcium FA show a noticeable reduction in surface abrasion resistance as a result of using FA concretes of high slump [25]. The lower surface abrasion resistance is explained due to the surface layer becoming rich in cement mortar and poor in coarse aggregate content. Note that the 30% low calcium FA concrete showed a higher slump of 160 mm, a 200% increase over that for the control concrete of similar w/b ratio. Thus, the large slump for the 30% FA concrete explains the high porosity of concrete, and the largest quantity of chloride at the surface (0–5 mm and 5–25 mm) of the slab.

The higher slump measured for the FA concrete is, in general, due to the lower water requirement for achieving a required degree of workability compared to that required for an equivalent concrete without FA. The FA derives the water reducing property by its ability to disperse the cement particles similar to an organic admixture [26]. Owing to its low CaO content, the Al_2O_3 in Class F fly ash preferentially reacts with the silicate to form crystalline aluminosilicates such as mullite, $3Al_2O_3.2SiO_2$ [27]. Therefore, there is no C_3A in Class F fly ash. As a result, the blended cement containing the Class F fly ash had a substantially lower C_3A content than the control portland cement. This also partly explains the high slump of FA concrete.

The 65% GGBFS concrete in comparison showed a relatively lower slump of 115 mm which may result in lower segregation and bleeding at the surface of the slab. This is in addition to the moderate filler action by the GGBFS due to its relatively finer particle size (417 m² kg⁻¹) compared to cement (345 m² kg⁻¹). On the other hand, the 10% SF slab, with the least slump of only 25 mm, coupled with its strong pozzolanic and filler action as a result of finer particle size, showed relatively less penetration of chloride at the surface compared to the slabs containing other mineral admixtures. For a given water content, the addition of SF would therefore decrease the slump of the mixture because of its finer particle size which increases the surface area. However, the concrete still retained its workability due to increase in the cohesiveness of the mixture. Thus, the 10% SF slab was the least affected as a result of the simple replacement of cement with mineral admixtures while maintaining 0.60 as the w/b ratio of the concrete mix.

While the chlorides diffuse through concrete, they are more likely to penetrate down to the level of the reinforcement steel through cracks. High w/b ratio concretes are more likely to crack, either due to imposed stresses, or through drying shrinkage, and effect of these on chloride penetration was not the subject of the present investigation. However, the importance of cracks in the overall scenario of the durability of concrete structures should not be underestimated, and these have been discussed in greater details [1–4].

Stability of Friedel's Salt and Ettringite

During the atmospheric carbonation of concrete, the carbon dioxide (CO_2) dissolves in pore water to form carbonic acid (H_2CO_3), which then reacts with $Ca(OH)_2$ to form the insoluble calcium carbonate ($CaCO_3$) as shown by the following equations.

$$CO_2 + H_2O \rightarrow H_2CO_3 \tag{1}$$

$$H_2CO_3 + Ca(OH)_2 \rightarrow CaCO_3 \downarrow + 2H_2O . \tag{2}$$

Calcium carbonate in a carbonated concrete is usually found in the form of the crystalline mineral calcite. On continuation of the above chemical reactions, the amount of portlandite in the cement paste diminishes, and this eventually will lead to a drop in the pH value of the pore water. Due to the continued atmospheric carbonation of field concrete structures, the alkalinity of the concrete can drop to as low a pH value as 8.5 or even lower [28].

In the present investigation, for the sample drawn at the 0–5 mm depth interval from the 30% FA slab, the DTA, and XRD results showed the absence of the portlandite, Friedel's salt, and ettringite, and the presence of a large amount of calcite. The phenolphthalein (1% in ethanol) spray test also indicated an average carbonation depth of 5 mm. The phenolphthalein solution used in the present investigation (1% in ethanol) indicates no coloration (carbonation) for the concrete at a pH below ≈11, and the concrete at a pH greater than ≈11 will become purple red (carbonation free). Thus, the results from the phenolphthalein spray test indicate that, due to the consumption of the entire portlandite, the concrete at the 0–5 mm depth interval attained a pH below 11.

As stated earlier, the average carbonation depths for the control slab (0.60 w/b ratio), 65% GGBFS slab, 10% SF slab, and the plain cement concrete slab (0.45 w/b ratio) were 3 mm, 2.5 mm, 1.25 mm, and 1.25 mm, respectively, which were lower than that for the 30% FA slab. The DTA results also showed relatively lower amounts of calcite at the 0–5 mm depth interval for the 65% GGBFS slab, 10% SF slab, and the control slab (0.60 w/b ratio) compared to that for the 30% FA slab. From the measured carbonation depths, it appears that a part of the concrete drawn at the 0–5 mm depth interval from the 65% GGBFS slab, 10% SF slab, and the plain cement concrete slab (0.60 and 0.45 w/b ratios) had a pH below 11, while the rest of it was at a relatively higher pH (more alkaline). Friedel's salt, portlandite, and ettringite present at the 0–5 mm depth interval are believed to be from that part of the concrete existing at a pH > 11 (more alkaline).

From the above discussion it is evident that the Friedel's salt formed due to the chemical interaction between the penetrating chlorides and the C_3A phase of the cement dissolves when the pH of the surrounding concrete drops below a value of 11. This is clearly demonstrated in the severely carbonated concrete drawn at the 0–5 mm depth interval from the 30% FA slab. Thus, the stability of the Friedel's salt is dependent on the pH of the concrete surrounding it. In the event of its dissolution in accordance with the equilibrium given below (3), the free-chloride ion concentration in the pore solution would be raised thus increasing corrosion risk to the reinforcement steel.

$$3CaO . Al_2O_3 . CaCl_2 . 10H_2O \Leftrightarrow 4Ca^{2+} + 2Cl^- + 6H^- + 2Al(OH)_3 + 4H_2O . \tag{3}$$
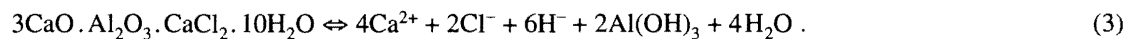
Page and Vennesland [29] also suggested the possibility of the dissolution of Friedel's salt in the event of decreased pH of the pore solution. Kayyali and Haque [30] have reported an increased free-chloride ion concentration in pore solution, when the 30% FA concrete admixed with $CaCl_2$ was carbonated; however, no mechanism for the increased free-chloride ion concentration was suggested.

Amongst the slabs containing mineral admixtures, though the 30% FA slab showed a greater tendency for the dissolution of Friedel's salt at the surface (0–5 mm), the reinforcement steel would still be safe from corrosion attack provided the structure is designed with an adequately thick cover. This is because the 30% FA concrete, as already shown earlier, offers a greater resistance to chloride penetration at higher depth intervals than the plain cement concrete slab of 0.45 w/b ratio.

Ettringite was also not evident in the concrete drawn at the 0–5 mm depth interval from the 30% FA slab; however, ettringite was clearly evident at greater depths. This suggests that the pH controls the stability of ettringite [31, 32]. Ettringite is known to be unstable below a pH around 10.5 to 10.7. This indirectly confirms that the pH value of the concrete at the 0–5 mm depth interval in the 30% FA slab was below the 10.5 to 10.7 pH range, as indicated by the phenolphthalein spray test.

Atmospheric Carbonation of Slabs

In the present investigation the atmospheric carbonation of the slabs would not be expected during the 7 day wetting period, as the air permeability of the concrete is unfavorable for the diffusion of atmospheric CO_2 through the concrete. The air permeability for concrete decreases with increasing relative humidity (RH), and the decrease is marked above 80% RH [28]. Later, during the 3 day air drying period, the capillary pores may become partly emptied and this may facilitate an enhanced diffusion rate for the CO_2 through the concrete cover, although it is very likely for the capillary pores to become completely empty during this period. Hence, there is a possibility for the slabs to carbonate during the drying period of the 10 day cycle; however, optimum carbonation occurs only when the RH of the concrete drops down to 50% [33]. Hence, it is most unlikely that the atmospheric carbonation will take place at an optimum rate throughout the 3 day drying period. There is also the possibility of re-alkalization due to cement hydration that might take place during the 7 day ponding as soon as the next 10 day cycle begins. Thus, significant carbonation of the slabs commences only after the completion of the 50 exposure cycles, or after the completion of the 500 days of indirect wet curing, and the carbonation continues during the time gap of one and half years. The carbonation recommences once again after the completion of the 70 exposure cycles, and continues until the beginning of the study reported here with a time gap of nearly two and half years. The chloride ions diffused through the concrete cover until the end of the 50 exposure cycles also assist in the subsequent carbonation process by retaining moisture, and thus avoiding the drying of the slabs. Thus, the higher carbonation of the concrete at the surface for the 30% FA slab cannot be due to lack of adequate long-term curing as the slabs were indirectly cured for 500 days after the initial 28 days curing.

The 30% FA slab showed the highest depth of carbonation (5 mm) compared to the other slabs due to the presence of porous concrete at the surface. There was no evidence from DTA and XRD results to show the formation of calcite in the concrete at the 5–25 mm depth interval to suggest the attack of atmospheric CO_2 on the concrete. However, the plain cement concrete slab of 0.60 w/b ratio showed an average carbonation depth of 3 mm, and this was the only slab to show the evidence through DTA to demonstrate the formation of a significant amount of calcite in the concrete at the 5–25 mm depth interval. Thus, over a similar period of exposure, the 30% FA slab showed a greater resistance to atmospheric CO_2 attack from the 5–25 mm depth interval onwards. Thus, despite the porous nature of the surface concrete, the carbonation depth of the 30% FA slab was limited to the surface concrete layer of 5 mm thickness, which apparently, was not representative of the whole concrete. The 10% SF slab was as good as the plain cement concrete slab of 0.45 w/b ratio (1.25 mm carbonation depth) against carbonation attack, while the 65% GGBFS slab was marginally inferior (2.5 mm carbonation depth) to the plain cement concrete slab of 0.45 w/b ratio. Thus, for all the slabs blended with mineral admixtures the carbonation depths were confined to the surface 0–5 mm concrete layer, which is not truly representative of the entire concrete.

The above results indicate that blended cement concrete structures of 0.60 w/b ratio are relatively more susceptible to deterioration from chlorides penetrating from an external environment than from atmospheric carbonation attack. However, concrete structures made with blended cements, even of 0.60 w/b ratio, will still delay the onset of chloride-induced corrosion on the reinforcement steel, provided they are designed with an adequate cover over the steel. The significance of these findings is not to be recommend the use of high w/b ratio mixes, even if they contain mineral admixtures for structures exposed to chloride-laden environments, but to highlight the significant benefits that can be derived by incorporating mineral admixtures in all concretes irrespective of their w/b ratios. For structures exposed to chloride attack, the current code requirements for relatively low w/b ratio mixes are sensible, and should be followed, since they lead to higher quality concretes.

CONCLUSIONS

The following conclusions are derived from a 6-year experimental study of concrete slabs exposed to chloride penetration and atmospheric carbonation.

1. Concrete slabs containing mineral admixtures (FA, GGBFS, and SF), but made with a relatively high w/b ratio of 0.60 were remarkably effective in resisting chloride penetration particularly beyond the 25–45 mm depth from the surface.

Although all these slabs showed large quantities of chloride in the top surface layers, except for the FA slab, these quantities were lower than those found in the plain cement concrete control slab with the same w/b ratio. They were, however, higher than those found in the surface layers of the plain cement concrete slab with 0.45 w/b ratio. The very high chloride concentration in the FA slab at the top is believed to be due to the increased slump of the FA concrete, and therefore the increased porosity of the surface layer. On the other hand, in plain cement concrete slab with 0.60 w/b ratio, significant proportions of chlorides had penetrated upto the 85–105 mm depth interval, in amounts much higher than that in the slabs with mineral admixtures.

2. It is concluded that concrete slabs of 0.60 w/b ratio and containing portland cement blended with mineral admixtures would be very effective in delaying the onset of reinforcement steel corrosion provided the structure is designed with an adequately thick cover.

3. The plain cement concrete slab of 0.60 w/b ratio indicated the progress of the carbonation front to the 5–25 mm depth. Despite the higher w/b ratio, the average carbonation depths for the 30% FA concrete, 65% GGBFS concrete and 10% SF concrete were 5 mm, 2.5 mm, and 1.25 mm respectively.

4. Concrete slabs of 0.60 w/b ratio made with mineral admixtures appear to be relatively more susceptible to chloride-induced deterioration than that arising from the atmospheric carbonation-induced deterioration.

5. Friedel's salt formed due to the interaction between the penetrating chlorides and the C_3A phase in the cement, decomposed when the alkalinity of the concrete dropped due to atmospheric carbonation. The 30% FA concrete of 0.60 w/b ratio was found to be relatively more prone to the dissolution of Friedel's salt present at the surface (0–5 mm) of the concrete.

6. Ettringite is unstable in severely carbonated concrete.

ACKNOWLEDGEMENTS

REFERENCES

[1]   R.N. Swamy, "Design — The Key to Concrete Material Durability and Structural Integrity", *Proc. International Conference on Reinforced Concrete Materials in Hot Climates, United Arab Emirates University*, vol. 1, 1994, pp. 3–36.

[2]   R.N. Swamy, "A Global Design Management Strategy to Enhance Corrosion-Free Durable Service Life of Concrete Constructions", *Journal of Chinese Corrosion Engineering*, 9(4) (1995), pp. 205–214.

[3]   R.N. Swamy, T. Oshiro, and S. Tanikawa, "Global Strategy to Enhance Service Life of Deteriorating Structures, and Extending the Life Span of Structures, *Proc. International Symposium on IABSE*, 1995, pp. 459–462.

[4]   R.N. Swamy, "High Performance and Durability Through Design", in *International Workshop on High Performance Concrete*. ed. Paul Zia. ACI Publ. SP-159, 1996, pp. 209–230.

[5]   P.K. Mehta, "Pozzolanic and Cementitious By-Products as Mineral Admixtures for Concretes — A Critical Review", *Proc. ACI/CANMET Publication, Quebec*, SP-79, vol. 1, 1983, pp. 1–46.

[6]   R.N. Swamy, "Fly Ash Concrete — Potential Without Misuse", *Materials and Structures*, 23 (1990), pp. 397–411

[7]   R.N. Swamy, "Fly Ash and Slag: Standards and Specifications — Help or Hindrance?", *Materials and Structures*, 26 (1993), pp. 600–613.

[8]   R.N. Swamy, ed., *Blended Cements in Construction*. London: Elsevier Applied Science, 1991.

[9]   K.W.J. Treadaway, R.N. Cox, and B.L. Brown, "Durability of Corrosion Resisting Steels in Concrete", *Proc. Institution of Civil Engineers*, Part 1, 86 (1989), pp. 305–311.

[10]   ASTM C 618-87, *Fly Ash and Raw Calcinated Natural Pozzolans for Use as a Mineral Admixture in Portland Cement Concrete*. 04.02, 1988, 291 pp.

[11]   BS 3892: Part 1, *Pulverised Fuel Ash for Use as a Cementitious Component in Structural Concrete*, 1982.

[12]   BS 1881: Part 124, *Determination of Chlorides Contents*, 1988, 17 pp.

[13]   Highway Research Board, "Guide to Compounds of Interest in Cement and Concrete Research", in *Special Report 127*. Washington D.C.: Highway Research Board, 1972, 28 pp.

[14]   C.L. Page, N.R. Short, and A. El Tarras, "Diffusion of Chloride Ions in Hardened Cement Paste", *Cement and Concrete Research*, 11(3) (1993), pp. 395–406.

[15] A.K. Suryavanshi, J.D. Scantlebury, and S.B. Lyon, "The Binding of Chloride Ions by Sulphate Resistant Portland Cement", *Cement and Concrete Research*, **25**(3) (1995), pp. 581–592.

[16] V.S. Ramachandran, *Calcium Chloride in Concrete*. London: Applied Science Publisher, 1976, 107 pp.

[17] H.F.W. Taylor, *Chemistry of Cements*. London: Academic Press, 1991, 177 pp.

[18] Z. Sauman, "Carbonation of Porous Concrete and Its Main Building Components", *Cement and Concrete Research*, **1**(6) (1971), pp. 645–662.

[19] H.E. Schwiete and U. Ludwig,, "Crystal Structure and Properties of Cement Hydration Products", in *Chemistry of Cements. Proc. 5th International Symposium, Tokyo*, 1968, pp. 37–67.

[20] V. Palik, "Corrosion of Hardened Cement Paste by Acetic and Nitric Acids, Part II: Formation and Chemical Composition of the Corrosion Products Layer", *Cement and Concrete Research*, **24**(8) (1994), pp. 1495–1508.

[21] L.H. Everett and K.W.J. Treadaway, "Deterioration Due to Corrosion in Reinforced Concrete", *Building Research Establishment Information Paper IP 12/80*, BRE Garston, 1980.

[22] P.K. Mehta, "Sulphate Resistance of Blended Portland Cements Containing Pozzolanic and Granulated Blast Furnace Slag", *Proc. Fifth International Symposium on Concrete Technology, Mexico*, 1981, pp. 35–50.

[23] R.F. Feldman, "Significance of Porosity Measurements on Blended Cement Performance", *Proc. ACI/CANMET Publication, Quebec*, SP-79, vol. 1, 1983, pp. 415–433.

[24] M. Collepardi, A. Marcialis, and R. Turriziani, "Penetration of Chloride Ions into Cement Pastes and Concrete", *Journal of American Ceramic Society*, **55**(10) (1972), pp. 534–535

[25] Electric Power Research Institute, "Investigation of High Volume Fly Ash Concrete System", *EPRI TR-1031*, October 1993, pp. 3–14.

[26] R. A. Helmuth, "Water-Reducing Properties of Fly Ash in Cement Pastes, Mortars and Concretes: Causes and Test Methods", *Proc. ACI Publication*, SP-91, vol. 1, 1986, pp. 171–199.

[27] P.K. Mehta, "Influence of Fly Ash Characteristics on the Strength of Portland — Fly Ash Mixtures", *Cement and Concrete Research*, **15**(4) (1985), pp. 669–674.

[28] O.E. Gjorv, "Mechanisms of Corrosion of Steel in Concrete Structures", *Proc. Evaluation of Materials 89, Kobe, Japan*, 1989, pp. 565–578.

[29] C.L. Page and O. Vennesland, "Pore Solution Composition and Chloride Binding Capacity of Silica Fume Cement Paste", *Materials and Constructions*, **16**(91) (1983), pp. 19–25

[30] O.A. Kayyali and M.N. Haque, "Effect of Carbonation on the Chloride Contamination in Pore Solution of Mortars With and Without Fly Ash", *Cement and Concrete Research*, **18**(4) (1988), pp. 636–648.

[31] D.Damidot and F.P.Glasser, "Thermodynamic Investigation of the $CaO-Al_2O_3-CaSO_4-H_2O$ System at 25°C and the Influence of Na_2O", *Cement and Concrete Research*, **23** (1993), pp. 221–238.

[32] A.Gabrisova, J. Havlica, and S.Sahu, "Stability of Calcium Sulphoaluminate Hydrate in Water Solutions with Various pH Values", *Cement and Concrete Research*, **21** (1991), pp. 1023–1027.

[33] L.J.Parrot, "Influence of Environmental Parameters upon Permeability: A Review. Permeability of Concrete as Criterion of its Durability", *Report of RILEM Technical Committee 116-PCW*, RILEM 1990.